Phase Stability and Sodium-Vacancy Orderings in a NaSICON Electrode

—Supporting Information—

Ziliang Wang,[1] Sunkyu Park,[2,3,4] Zeyu Deng,[1] Dany Carlier, [3,4] Jean-Noël Chotard,[2,4,#] Laurence Croguennec,[3,4] Gopalakrishnan Sai Gautam,[5] Anthony K. Cheetham,[1,6] Christian Masquelier,[2,4] Pieremanuele Canepa[1,7,*]

[1]Department of Materials Science and Engineering, National University of Singapore, 9 Engineering Drive 1, 117575, Singapore
[2]Laboratoire de Réactivité et de Chimie des Solides (LRCS), CNRS UMR 7314, Université de Picardie Jules Verne, 80039 Amiens Cedex, France
[3]CNRS, Univ. Bordeaux, Bordeaux INP, ICMCB, UMR CNRS 5026, F-33600, Pessac, France
[4]RS2E, Réseau Français sur le Stockage Electrochimique de l'Energie, FR CNRS 3459, F-80039 Amiens Cedex 1, France
[5]Department of Materials Engineering, Indian Institute of Science, Bengaluru, 560012, Karnataka, India
[6]Materials Department and Materials Research Laboratory, University of California, Santa Barbara, California 93106, USA
[7]Department of Chemical and Biomolecular Engineering, National University of Singapore, 4 Engineering Drive 4, 117585 Singapore, Singapore

Corresponding authors: [#]jean-noel.chotard@u-picardie.fr , [*]pcanepa@nus.edu.sg

S1. Density Functional Theory Calculations of $Na_XV_2(PO_4)_3$

In the reminder of this document the NaSICON material $Na_XV_2(PO_4)_3$ will be referred as N_XVP.

S1-1. Lattice parameters and structures of N_XVP ground states

Table S1 Fractional coordinates of atoms within each ground-state ordering (N_1VP, N_2VP, N_3VP, N_4VP) of NaSICON as computed by SCAN+*U*.

N_1VP				**N_2VP**			
Na	0.500090	0.500026	0.499881	Na	0.499979	0.500126	0.499948
Na	0.000194	0.999900	0.999997	Na	0.999966	0.000008	0.000001
V	0.643531	0.643161	0.641416	Na	0.613554	0.247955	0.893272
V	0.143582	0.141311	0.143227	Na	0.386436	0.752072	0.106755
V	0.356334	0.356868	0.358660	V	0.647049	0.640379	0.643888
V	0.856446	0.858625	0.856852	V	0.140362	0.144156	0.149926
P	0.249946	0.537169	0.962668	V	0.352949	0.359682	0.356101
P	0.961382	0.250306	0.537604	V	0.859593	0.855845	0.850079
P	0.538668	0.962574	0.249749	P	0.245392	0.545774	0.966538
P	0.461350	0.037483	0.750211	P	0.959945	0.247939	0.542380
P	0.750062	0.462756	0.037333	P	0.532993	0.956025	0.249744
P	0.038567	0.749685	0.462426	P	0.467005	0.043995	0.750221
O	0.869278	0.704448	0.495844	P	0.754615	0.454205	0.033502
O	0.497020	0.871322	0.704646	P	0.039992	0.752018	0.457630
O	0.708184	0.493030	0.870224	O	0.880021	0.698598	0.498178
O	0.997173	0.205447	0.370814	O	0.502242	0.854063	0.750450
O	0.369284	0.996451	0.204105	O	0.718255	0.456843	0.876644
O	0.208056	0.370642	0.992255	O	0.009505	0.179740	0.381755
O	0.130606	0.295845	0.504041	O	0.377730	0.966726	0.204707
O	0.502663	0.128903	0.295189	O	0.211782	0.363849	0.025359
O	0.291615	0.507366	0.129647	O	0.119970	0.301290	0.501728
O	0.002735	0.794412	0.629298	O	0.497920	0.145899	0.249503
O	0.630745	0.003353	0.796071	O	0.281835	0.543131	0.123362
O	0.791668	0.629337	0.007996	O	0.990444	0.820199	0.618236
O	0.774757	0.421747	0.556593	O	0.622249	0.033338	0.795252
O	0.558242	0.774623	0.419808	O	0.788302	0.636081	0.974697
O	0.422212	0.561550	0.775512	O	0.771634	0.409394	0.553705
O	0.058294	0.919835	0.274603	O	0.550624	0.787934	0.428807
O	0.275055	0.056086	0.921879	O	0.420932	0.548271	0.782437
O	0.922325	0.275355	0.061559	O	0.065791	0.914793	0.265303
O	0.225189	0.578197	0.443517	O	0.274425	0.079003	0.919167
O	0.441974	0.225372	0.580173	O	0.921544	0.275139	0.071014
O	0.577956	0.437850	0.224578	O	0.228303	0.590566	0.446302
O	0.941952	0.080095	0.725346	O	0.449319	0.212098	0.571148
O	0.724976	0.944058	0.078104	O	0.579059	0.451785	0.217589
O	0.077766	0.724685	0.938048	O	0.934130	0.085156	0.734713
				O	0.725550	0.920974	0.080775

				O	0.078466	0.724827	0.929041

N_3VP				N_4VP			
Na	0.508358	0.520398	0.473032	Na	0.500394	0.499966	0.499615
Na	0.008026	0.973669	0.019874	Na	0.000011	0.000360	0.999611
Na	0.249906	0.889139	0.618883	Na	0.251144	0.882101	0.616106
Na	0.615045	0.248978	0.878715	Na	0.615031	0.250504	0.883187
Na	0.115077	0.378903	0.748881	Na	0.885199	0.618362	0.248126
Na	0.749860	0.119149	0.389060	Na	0.118404	0.385126	0.748155
V	0.642684	0.643899	0.646102	Na	0.750559	0.114990	0.383249
V	0.142580	0.146019	0.144093	Na	0.382048	0.751286	0.116048
V	0.359385	0.359118	0.349256	V	0.645551	0.644738	0.645072
V	0.859500	0.849310	0.858844	V	0.144654	0.145622	0.145100
P	0.246064	0.539231	0.952964	V	0.355547	0.354480	0.354726
P	0.954651	0.254100	0.540850	V	0.854524	0.855478	0.854738
P	0.547487	0.962991	0.251395	P	0.249654	0.549326	0.950317
P	0.454738	0.040691	0.754013	P	0.952452	0.249537	0.548361
P	0.746215	0.452846	0.039133	P	0.548080	0.951339	0.250952
P	0.047583	0.751313	0.462974	P	0.451274	0.048062	0.750963
O	0.873367	0.710141	0.518880	P	0.749551	0.452485	0.048344
O	0.478837	0.880762	0.707344	P	0.049343	0.749635	0.450339
O	0.688599	0.475050	0.886726	O	0.889857	0.696457	0.482446
O	0.978908	0.207236	0.380868	O	0.483328	0.886880	0.699668
O	0.372843	0.018267	0.211148	O	0.696755	0.485111	0.888237
O	0.188877	0.386574	0.975336	O	0.984994	0.196663	0.388369
O	0.123876	0.291438	0.509432	O	0.386863	0.983555	0.199592
O	0.534356	0.117559	0.299881	O	0.196333	0.389944	0.982449
O	0.305498	0.482341	0.115396	O	0.113620	0.299725	0.517762
O	0.034366	0.800122	0.617467	O	0.514226	0.109955	0.306850
O	0.624430	0.009203	0.790774	O	0.301131	0.517092	0.110977
O	0.805709	0.615049	0.982234	O	0.017138	0.801065	0.611011
O	0.769932	0.416658	0.567292	O	0.609923	0.014074	0.806910
O	0.558710	0.779719	0.418490	O	0.799826	0.613559	0.017798
O	0.409964	0.560403	0.765375	O	0.769305	0.409921	0.565998
O	0.058078	0.918531	0.279791	O	0.567482	0.767080	0.409541
O	0.270369	0.067163	0.916902	O	0.409469	0.566241	0.767342
O	0.910279	0.265317	0.060039	O	0.066381	0.909388	0.267325
O	0.225267	0.581016	0.441199	O	0.266993	0.067610	0.909476
O	0.435046	0.227561	0.587700	O	0.909833	0.269262	0.066069
O	0.589385	0.434964	0.229250	O	0.233630	0.590031	0.431957
O	0.935286	0.087710	0.727729	O	0.435852	0.230646	0.590919
O	0.724783	0.941418	0.080717	O	0.590224	0.432517	0.231611
O	0.089125	0.729303	0.935218	O	0.932455	0.090261	0.731669
				O	0.730680	0.935745	0.090990
				O	0.090126	0.733666	0.931868

Table S2 Lattice constants (in Å and °), volumes (in $Å^3$) and space groups (Spg.) of the low-temperature-stable N_xVP orderings at low temperature, namely N_1VP, N_2VP, N_3VP, $N_{3.5}VP$ and N_4VP computed with SCAN+*U*. Note that Na intercalation in fully charged N_1VP forms the fully discharged phase, N_4VP, resulting in a volume expansion of ~9.8 %.

Structure	***a***	***b***	***c***	***α***	***β***	***γ***	**V / f.u.**	**Spg.**
N_1VP	8.473	8.473	21.169	90.000	90.000	120.000	219.499	$R\bar{3}c$
N_2VP	8.521	8.613	8.629	60.350	61.055	60.540	227.159	$P\bar{1}$
N_3VP	15.038	8.729	8.689	90.000	124.709	90.000	234.409	Cc
$N_{3.5}VP$	8.672	8.694	15.202	91.110	105.621	118.923	237.715	$P\bar{1}$
N_4VP	8.935	8.935	20.904	90.000	90.000	120.000	241.012	$R\bar{3}c$

Table S3 Computed average (Avg.) V-O bond lengths (in Å) of different VO_6 octahedra represented by their V oxidation states within N_1VP, N_2VP, N_3VP, $N_{3.5}VP$, and N_4VP. The bond lengths are averaged over all the specific octahedra within each N_xVP ordering. In N_1VP and N_2VP, which contain V(IV), the minimum (Min.) and maximum (Max.) V(IV)-O bond lengths are listed instead.

Structure	**Avg. V-O bond length of**		
	$V(II)O_6$	**$V(III)O_6$**	**$V(IV)O_6$**
N_1VP	—	—	Min. 1.855; Max. 1.959
N_2VP	—	2.003	Min. 1.818; Max. 2.038
N_3VP	—	2.012	—
$N_{3.5}VP$	2.057 for $V(II)/V(III)O_6$; 2.015 for $V(III)O_6$		
N_4VP	2.062 for $V(II)/V(III)O_6$		

S1-2. Electronic Structure of N_XVP

Figure S1 shows the SCAN+*U* calculated density of states (DOS) for the four thermodynamic ground-state structures.

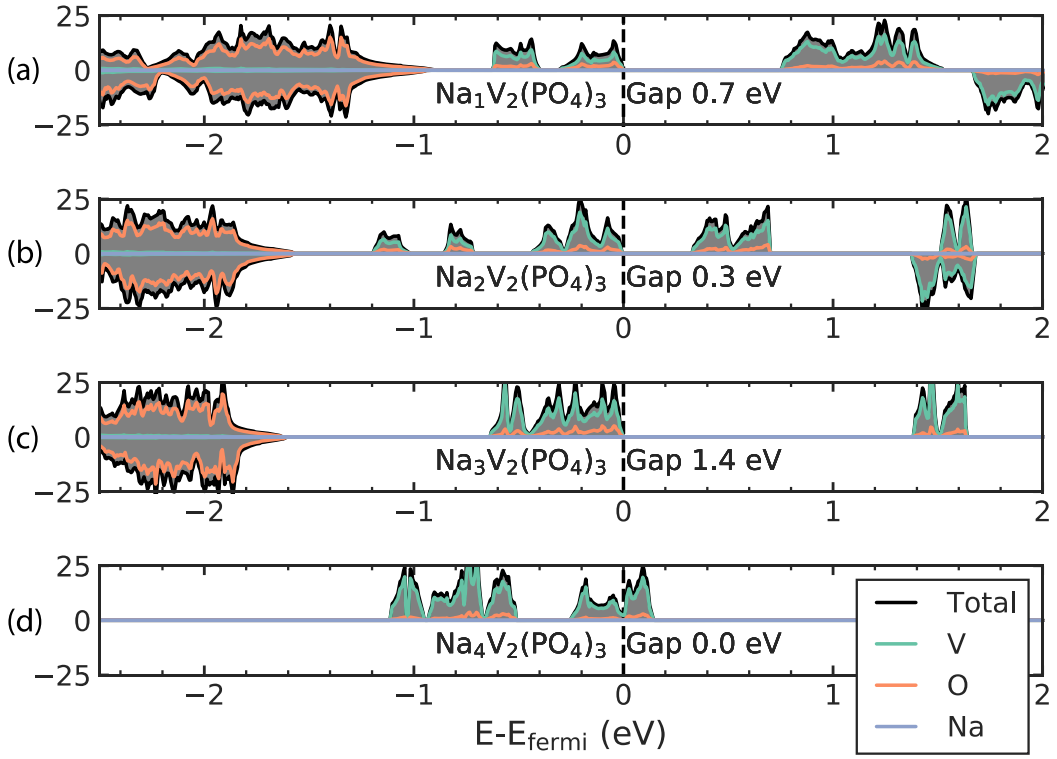

Figure S1 The total (gray) and element-projected (green for V, orange for O, blue for Na) DOS of the most stable $Na_xV_2(PO_4)_3$ phases. Na contents vary from x=1 (panel (a)) to x=4 (panel (d)). The vertical dashed lines denote the Fermi energy level, and the band gap is calculated from SCAN+U based DFT.

From **Figure S1,** we deduce that the vanadium 3*d* states dominate the valence band, and the band gap for N_1VP, N_2VP, N_3VP and N_4VP is 0.7 eV, 0.3 eV, 1.4 eV, and 0 eV, respectively.

Except for N_3VP where the gap opens due to the stabilization induced by the rhombohedral-to-monoclinic distortion, the band gap generally narrows as Na intercalation progresses from x = 1 to 4.

Figure S2 shows the spin-polarized DOS projected onto the 3d orbitals of vanadium in N_3VP.

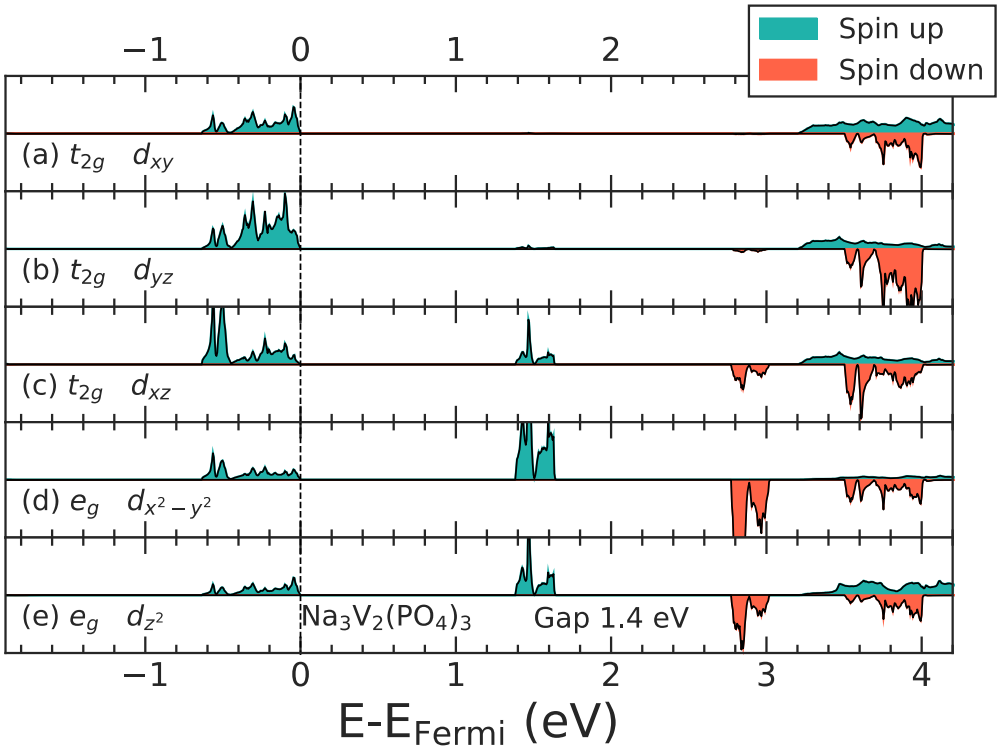

Figure S2 The projected DOS onto the 3d orbitals of vanadium in N_3VP. Panels (a) to (c) show the t_{2g} orbitals of vanadium (i.e., d_{xy}, d_{xz}, and d_{yz}) at valence band, and panels (d) and (e) show the e_g orbitals (i.e., d_{z^2}, and $d_{x^2-y^2}$) which are corresponding to the conduction band.

Figure S3 shows the band structure of N_4VP, where only 4 bands populate the Fermi energy level.

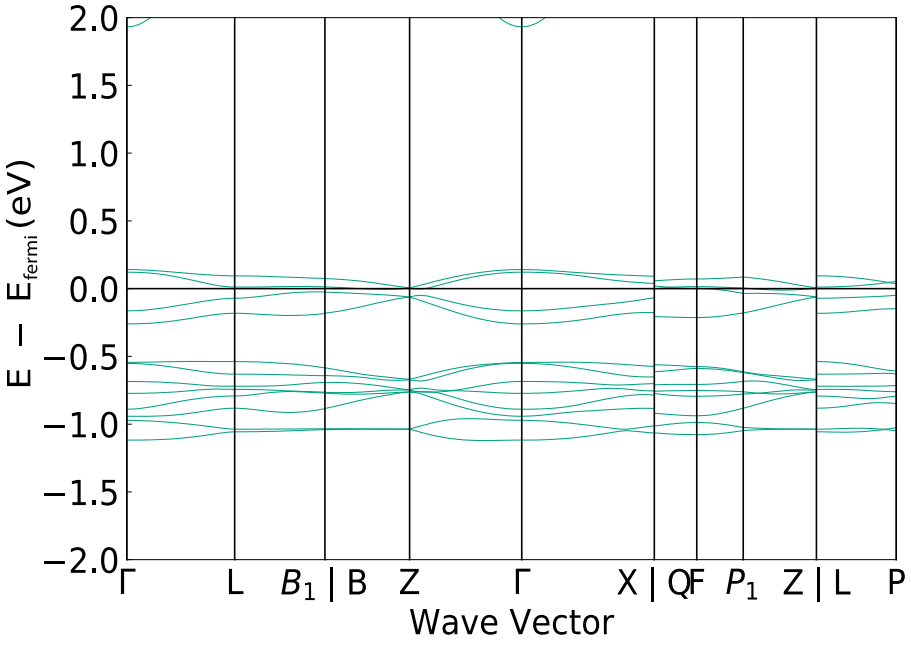

Figure S3 The band structure of $Na_4V_2(PO_4)_3$ computed from SCAN+*U* DFT calculation. The x axis shows the high symmetry K-point path, and the Fermi energy level is represented by the black horizontal line.

In **Table S4**, we list the computed average magnetic moments on the vanadium sites in N_1VP, N_2VP, N_3VP, $N_{3.5}VP$, and N_4VP, and assign the corresponding vanadium oxidation states.

Table S4 The DFT-computed magnetic moments (in μ_B) of vanadium sites within the NaSICON structures and assigned oxidation states.

Compound	**Oxidation States and Computed Magnetic Moments**		
	V(II)	**V(III)**	**V(IV)**
N_1VP	—	—	μ_B = 1.0
N_2VP	—	μ_B = 1.8	μ_B = 1.1
N_3VP	—	μ_B = 1.9	—
$N_{3.5}VP$	μ_B = 1.9-2.3		—
N_4VP	μ_B = ~2.3		—

Our DFT data demonstrates that the intercalation of Na ions into the N_1VP is realized by the reduction of V(IV) to V(III) to form N_3VP. Specifically, N_1VP and N_3VP are identified by a single vanadium oxidation state, namely V(IV) in N_1VP and V(III) in N_3VP, while the charge ordering on vanadium sites in N_2VP is clearly indicated by the distinct magnetic moments exhibited by V(IV) and V(III) ions. Further Na^+ intercalation into N_3VP gives rise to $N_{3.5}VP$ and N_4VP, accompanied by the appearance of a fractional V oxidation state of 2.5, due the metallic transformation (see **Figures S1** to **S3**) and consequent delocalization of 3*d* electrons on vanadium sites. Thus, we obtained average magnetic moments ranging from 1.9 μ_B to 2.3 μ_B (per vanadium), which are represented by the mixed states of V(III) and V(II).

S2. Cluster Expansion model

S2-1. General Theory of Cluster Expansion

We developed a CE Hamiltonian to parameterize the mixing energies ($E_{mixing}(\sigma)$ in **Eq. 7**) calculated from DFT (see **Section S1**) of various Na/vacancy orderings. The fitting of the CE was performed using the cluster assisted statistical mechanics (CASM) package.[1–4] The CE Hamiltonian was mapped onto a fixed prototypical structure, which we chose to be N_4VP (see **Section S2-2**), and we wrote the CE as a truncated summation of effective cluster interactions (ECIs) composed of pair, triplet, and quadruplet clusters according to **Eq. 1**.

$$E_{mixing}(\sigma) = \sum_{\alpha} J_{\alpha}\Phi_{\alpha}(\sigma) = \sum_{\alpha} J_{\alpha}\mathrm{m}_{\alpha}\prod_{i\in\beta}(\sigma_i) \quad (1)$$

where $E_{mixing}(\sigma)$ is the mixing energy as a function of Na/vacancy ordering (σ). Each term in the sum is written by the product of the ECI (J_{α}) of cluster α and its cluster function $\left(\Phi_{\alpha}(\sigma)\right)$, which incorporates the multiplicity of the cluster (m_{α}) and the correlation matrix ($\prod(\sigma)$) averaged over all clusters β that are symmetrically equivalent to α. Based on the Chebyshev definition, each Na site occupied by Na ion assumes $\sigma_{\mathrm{i}} = -1$ and each vacancy assumes $\sigma_{\mathrm{i}} = +1$. Φ_{α} was generated within a radius of 10, 6, and 5 Å for the pairs, triplets, and quadruplets, respectively.

To evaluate the accuracy and predictability of the CE against the DFT mixing energy, the root mean squared error (RMS) and the leave-one-out cross-validation scores (LOOCV) were simultaneously minimized using the compressive sensing algorithm. [5] Specifically, we used a value of $\alpha = 1 \times 10^{-4}$ to penalize the L1 norm consisting of the magnitude of all ECIs and the RMS of fitted energies.[5]

S2-2. Cluster Expansion model topology of N_XVP

Table S5 shows the atom types and coordinates of the N_4VP rhombohedral structure, on which the CE model is developed to map the various Na/vacancy orderings. The lattice parameters of the N_4VP structure ($R\bar{3}c$) are *a = b = 8.936 Å, c = 20.92 Å, α = β = 90°, γ= 120°.* Note that the coordinates listed below have not been optimized with DFT.

Table S5 Atom sites and fractional coordinates of the model topology cell of N_4VP. Na(1) and Na(2) sites for Na ions to occupy are consistent with the labels indicated **in Figure 1** of the main article.

Atom Site	Site Index and type	x	y	z
Na/Va	0 Na(1)	0.500001	0.500001	0.500001
Na/Va	1 Na(1)	0.000001	0.000001	0.000001
Na/Va	2 Na(2)	0.116602	0.749998	0.383415
Na/Va	3 Na(2)	0.749998	0.383415	0.116602
Na/Va	4 Na(2)	0.383415	0.116602	0.749998
Na/Va	5 Na(2)	0.616602	0.883415	0.249998
Na/Va	6 Na(2)	0.883415	0.249998	0.616602
Na/Va	7 Na(2)	0.249998	0.616602	0.883415
V	8	0.353862	0.353862	0.353862
V	9	0.853862	0.853862	0.853862
V	10	0.646141	0.646141	0.646141
V	11	0.146141	0.146141	0.146141
P	12	0.450427	0.750001	0.049581
P	13	0.750001	0.049581	0.450427
P	14	0.049581	0.450427	0.750001
P	15	0.950427	0.549581	0.250001
P	16	0.549581	0.250001	0.950427
P	17	0.250001	0.950427	0.549581
O	18	0.301094	0.111477	0.517259
O	19	0.111477	0.517259	0.301094
O	20	0.517259	0.301094	0.111477
O	21	0.801094	0.017259	0.611477
O	22	0.017259	0.611477	0.801094
O	23	0.611477	0.801094	0.017259
O	24	0.698911	0.888527	0.482756
O	25	0.888527	0.482756	0.698911
O	26	0.482756	0.698911	0.888527
O	27	0.198911	0.982756	0.388527
O	28	0.982756	0.388527	0.198911
O	29	0.388527	0.198911	0.982756
O	30	0.589832	0.232484	0.432262
O	31	0.232484	0.432262	0.589832
O	32	0.432262	0.589832	0.232484
O	33	0.089832	0.932262	0.732485
O	34	0.932262	0.732484	0.089832
O	35	0.732484	0.089832	0.932262
O	36	0.41017	0.767523	0.567745
O	37	0.767523	0.567745	0.41017
O	38	0.567745	0.41017	0.767523
O	39	0.91017	0.067745	0.267523

O	40	0.067745	0.267523	0.91017
O	41	0.267523	0.91017	0.067745

S2-3. Model fitting results

Figure S4 plots the formation (mixing) energies vs. Na compositions generated by CE (red) and DFT (blue). The corresponding error of CE model against DFT are also shown.

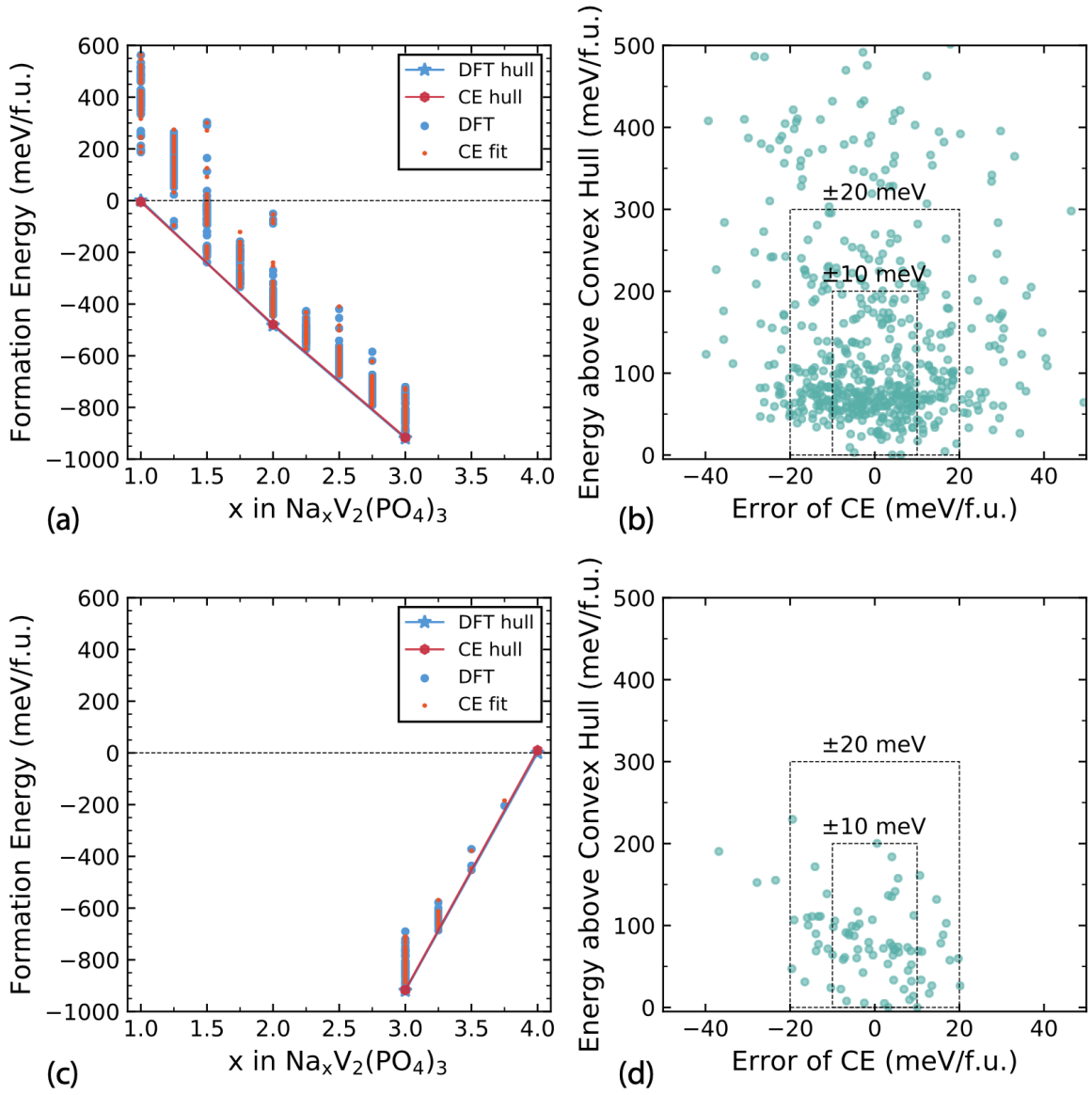

Figure S4 DFT and CE predicted formation (mixing) energies N_xVP. The convex hulls with solid red line. Panel (a) shows the mixing energies of N_xVP (range $1 \leq x \leq 3$) vs. Na content (x), and the corresponding error of the CE model is shown in panel (b). Panels (c) and (d) depict the mixing energies vs. Na contents (range $3 \leq x \leq 4$) and the error of the CE model, respectively. In panels (a) and (c), DFT and CE convex hulls are shown by solid blue (not visible) and red lines, where blue stars and red hexagons indicate the stable configurations forming the convex hull line. Blue and red dots depict the mixing energies of unstable configurations from DFT and the CE model respectively. In panels (b) and (d), the dashed lines denote the confidence intervals (of ± 10 and ± 20 meV/f.u.) of the CE models.

Separate CE models are fitted in the Na composition range $1 \leq x \leq 3$ (**Figure S4**(a)) and $3 \leq x \leq 4$ (**Figure S4**(c)), respectively, resulting in two sets of ECIs. The separation of the CE fitting is due to the differences between the electronic structure of the Na-poor (semiconducting) and Na-rich (metallic) regions of N_xVP (see **Section S1-3**). Based on panels (a) and (c) of **Figure S4**, our CE models well reproduced the DFT-calculated ground state configurations, i.e., N_1VP, N_2VP, N_3VP, and N_4VP. Specifically, the RMS and LOOCV errors of the CE model for $1 \leq x \leq 3$ is ~14.85 meV/f.u. (~0.71 meV/atom), and ~22.4 meV/f.u. (~1.07 meV/atom), respectively. For $3 \leq x \leq 4$, the RMS and LOOCV of CE were ~11.45 meV/f.u. (~0.55 meV/atom), and ~18.9 meV/f.u. (~0.9 meV/atom), respectively.

To further quantify the accuracy of our CE models, the errors of the CE are shown in panels (b) and (d) of **Figure S4**. The plotted error values are the differences between the CE-predicted and corresponding DFT-calculated E_{mixing} for $1 \leq x \leq 3$ (panel (b)), and $3 \leq x \leq 4$ (panel (d)), respectively.

S2-4. Analysis of the Effective Cluster Interactions

Table S6 lists the 33 distinctive effective cluster interactions (ECIs) of our CE model fitted in the composition region N_1VP–N_3VP.

Table S6. ECIs for CE model fitted on Na composition region $1 \leq x \leq 3$ of N_xVP. Site refers to the site labelled in **Table S5**. Min. and Max. show the minimum and maximum lengths of each ECI term, respectively, and multi. is the multiplicity of each cluster. The reference cell is labelled as [0, 0, 0].

Cluster type	Index	Site	Cell	Min. (Å)	Max. (Å)	ECI (meV)	ECI/multi. (meV)
Point tems	2	4	[0, 0, 0]	—	—	1655.913	275.986
	3	0	[0, 0, 0]	—	—	916.37	458.185
Pair Terms	4	4//0	[0, 0, 0] [0, 0, 0]	3.334	3.334	234.366	39.061
	5	4//1	[0, 0, 0] [0, 0, 1]	3.334	3.334	265.402	44.234
	6	4//6	[0, 0, 0] [-1, 0, 0]	4.498	4.498	31.386	5.231
	8	4//5	[0, 0, 0] [0, -1, 0]	4.812	4.812	–26.142	–4.357
	9	4//2	[0, 0, 0] [0, 0, 0]	4.922	4.922	14.415	2.403
	11	4//2	[0, 0, 0] [1, -1, 0]	5.674	5.674	15.998	2.666
	14	0//1	[0, 0, 0] [1, 0, 0]	6.227	6.227	18.582	3.097
	17	4//5	[0, 0, 0] [0, 0, 0]	6.668	6.668	–11.809	–1.968
	18	4//2	[0, 0, 0] [0, -1, 0]	6.992	6.992	100.595	16.766
	25	4//5	[0, 0, 0] [-1, 0, 0]	8.109	8.109	–13.176	–2.196
	31	4//4	[0, 0, 0] [0, -1, 0]	8.674	8.674	–208.75	–34.792
	32	4//4	[0, 0, 0] [-1, 0, 0]	8.674	8.674	–206.17	–34.362
	33	0//0	[0, 0, 0] [0, 0, -1]	8.674	8.674	–87.795	–14.632
	34	4//4	[0, 0, 0] [0, 0, -1]	8.674	8.674	–40.975	–6.829
	35	4//3	[0, 0, 0] [0, -1, 0]	8.841	8.841	14.931	2.489
	37	4//7	[0, 0, 0] [1, -1, -1]	8.875	8.875	–10.004	–1.667
	38	4//6	[0, 0, 0] [-1, -1, 1]	8.875	8.875	–21.766	–3.628
	39	4//4	[0, 0, 0] [1, -1, 0]	8.936	8.936	169.372	28.229
	43	4//5	[0, 0, 0] [1, -1, 0]	9.038	9.038	–3.663	–0.61
	46	4//1	[0, 0, 0] [1, 1, 0]	9.416	9.416	–41.499	–6.917

	49	4//0	[0, 0, 0] [-1, -1, 1]	9.416	9.416	–29.701	–4.95
Triplet Terms	51	4//6//1	[0, 0, 0] [-1, 0, 0] [0, 0, 1]	3.334	4.498	22.742	3.79
	53	4//0//2	[0, 0, 0] [0, 0, 0] [0, 0, 0]	3.334	4.922	–19.119	–3.187
	55	4//5//3	[0, 0, 0] [0, -1, 0] [0, 0, 0]	4.498	4.922	–12.501	–2.084
	57	4//2//1	[0, 0, 0] [0, -1, 1] [0, 0, 1]	3.333	4.922	–63.981	–10.664
	59	4//5//7	[0, 0, 0] [0, -1, 0] [0, -1, 0]	4.498	4.922	–23.974	–3.996
	60	4//2//3	[0, 0, 0] [0, -1, 1] [-1, 0, 1]	4.922	4.922	–14.025	–7.013
	61	4//5//6	[0, 0, 0] [0, -1, 0] [-1, 0, 0]	4.498	5.674	–15.809	–2.635
	62	4//5//2	[0, 0, 0] [0, -1, 0] [1, -1, 0]	4.498	5.674	–13.268	–2.211
Quadruplet Terms	66	4//0//2//3	[0, 0, 0] [0, 0, 0] [0, 0, 0]	3.334	4.922	31.171	15.586
	68	4//2//3//1	[0, 0, 0] [0, 0, 0] [0, -1, 1] [-1, 0, 1] [0, 0, 1]	3.334	4.922	5.385	2.693

Table S7 reports the 20 distinctive ECIs in the CE model fitted on N_3VP–N_4VP region.

Table S7 ECIs of CE model fitted on Na composition region $3 \leq x \leq 4$ of N_xVP.

cluster type	index	site	cell	Min. (Å)	Max. (Å)	ECI (meV)	ECI/multi. (meV)
Point Terms	2	4	[0, 0, 0]	—	—	–527.5	–87.917
	3	0	[0, 0, 0]	—	—	136.003	68.001
Pair Terms	4	4//0	[0, 0, 0] [0, 0, 0]	3.333	3.333	772.842	128.807
	6	4//6	[0, 0, 0] [-1, 0, 0]	4.498	4.498	81.938	13.656
	7	4//7	[0, 0, 0] [0, -1, 0]	4.498	4.498	108.13	18.022
	8	4//5	[0, 0, 0] [0, -1, 0]	4.812	4.812	58.163	9.694
	9	4//2	[0, 0, 0] [0, 0, 0]	4.922	4.922	104.309	17.385
	10	4//2	[0, 0, 0] [0, -1, 1]	4.922	4.922	173.898	28.983
	11	4//2	[0, 0, 0] [1, -1, 0]	5.674	5.674	74.069	12.345
	18	4//2	[0, 0, 0] [0, -1, 0]	6.992	6.992	122.151	20.358
	22	4//0	[0, 0, 0] [-1, 0, 0]	7.706	7.706	109.077	18.179
	32	4//4	[0, 0, 0] [-1, 0, 0]	8.674	8.674	–10.286	–1.714
	40	4//4	[0, 0, 0] [0, 1, -1]	8.936	8.936	3.172	0.529
	42	4//4	[0, 0, 0] [1, 0, -1]	8.936	8.936	1.11	0.185
Triplet Terms	53	4//0//2	[0, 0, 0] [0, 0, 0] [0, 0, 0]	3.334	4.922	–79.109	–13.185
	60	4//2//3	[0, 0, 0] [0, -1, 1] [-1, 0, 1]	4.922	4.922	–2.09	–1.045
	62	4//5//2	[0, 0, 0] [0, -1, 0] [1, -1, 0]	4.498	5.674	13.296	2.216
	64	4//2//3	[0, 0, 0] [1, -1, 0] [0, -1, 1]	5.674	5.674	–5.466	–2.733
Quadruplet Terms	65	4//7//6//1	[0, 0, 0] [0, -1, 0] [-1, 0, 0] [0, 0, 1]	3.334	4.922	–26.638	–4.44
	67	4//7//2//1	[0, 0, 0] [0, -1, 0] [0, -1, 1] [0, 0, 1]	3.334	4.922	–4.215	–4.036

Figure S5 plots the relevant most significant ECIs (normalized by their multiplicities) as a function of their cluster index.

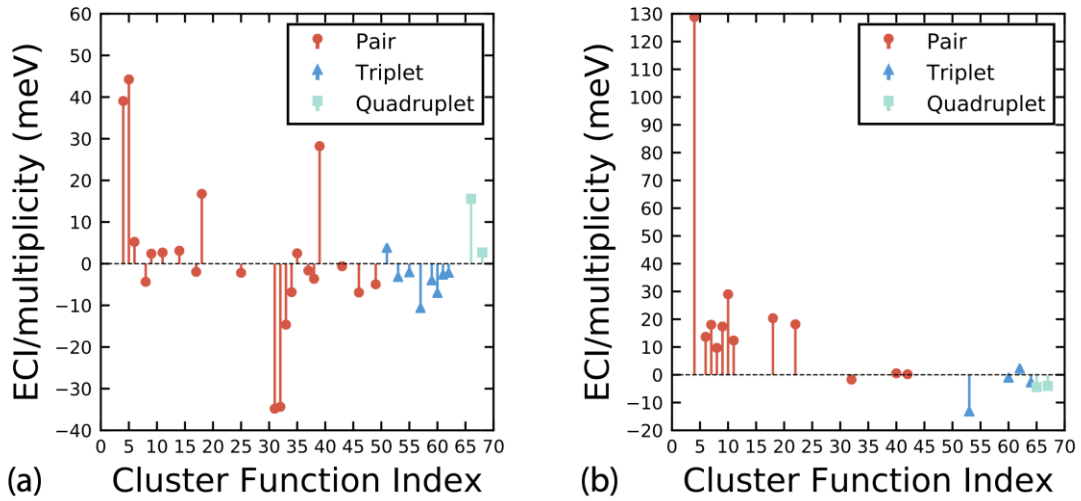

Figure S5 Normalized ECIs vs. their cluster function index identified during the CE fitting. ECIs for the CE in the Na composition range (a) 1 ≤ x ≤ 3 and (b) 3 ≤ x ≤ 4.

For the CE model fitted on Na composition region $1 \leq x \leq 3$ (of **Table S6** and **Figure S5**(a)), out of the 33 clusters, 21 are pairs, 8 are triplets and 2 are quadruplets, where the pairs are the most dominant in terms of ECI/multiplicity (red dots in **Figure S5(a)**). The pairs #31 and #32 are the most stabilizing term for like-species (i.e., Na-Na or vacancy-vacancy) with ECI/multiplicity of –34.792 meV and –34.362 meV, respectively. In contrast, pairs #4 (~39.061 meV) and #5 (~44.234 meV) have a significantly stabilizing contribution for unlike-species (i.e., Na-vacancy) in our model. For the CE model fitted on Na composition range $3 \leq x \leq 4$ (of **Table S7** and **Figure S5(b)**), out of the 20 clusters, 12 are pair interactions, 4 are triplets and 2 are quadruplets, respectively. The most significant pair is #4 (~128.807 meV), which stabilizes Na-vacancy configurations.

S3. Monte Carlo simulations

S3-1. Methodology

We used the CASM package to perform the grand-canonical Monte Carlo (gcMC) simulations[6] on $16 \times 16 \times 16$ supercells of the primitive rhombohedral structure. The gcMC runs ranged between 32,768,000 and 327,680,000 steps and were conducted independently in three composition regions of N_1VP–N_2VP, N_2VP–N_3VP, and N_3VP–$N_{3.5}VP$–N_4VP.

S3-2. Thermodynamic integration

The gcMC simulations were performed for N_XVP system in the chemical potential (μ) and temperature (T) space, and were then converted into (T, x) space to define the phase boundaries in **Figure 2**. Based on the 2 separate CE fits discussed in **Section S2**, our gcMC using CE model fitted for the composition region N_1VP–N_3VP started from T = 10 K to 1600 K with a step of 1 K at μ = –4.5, –3.6, and –2.5 eV/f.u., corresponding to N_1VP, N_2VP, and N_3VP, respectively. At every *T*, μ was scanned in both forward (μ = –4.5 and –3.6 eV/f.u.) and backward (μ = –3.6 and –4.5 eV/f.u.) directions with a step of 0.01 eV/f.u. to cover the relevant Na composition regions. Similarly, the gcMC using CE model fitted for N_3VP-N_4VP scanned at the same temperature interval at μ = 6.5, 7.2, and 9.5 eV/f.u., indicated by N_3VP, $N_{3.5}VP$, and N_4VP, respectively.

The phase boundaries were identified by the lowest envelopes of the grand-canonical potential (ϕ) of each stable phase. ϕ was computed as in **Eq. 2**,

$$\phi = E - TS - \mu x \tag{2}$$

where E is the energy calculated from CE model, T is the temperature, S is the configurational entropy, μ is the Na chemical potential, and x represents the Na composition in N_xVP. To remove the numerical hysteresis for gcMC, which might cause the different voltage curves while simulating along charging/discharging process, we performed the thermodynamic integration.[7] At fixed μ and variable T, ϕ was calculated using **Eq. 3**,

$$\phi(\beta,\mu) = \frac{\beta_0}{\beta}\phi_0(\beta_0,\mu) + \frac{1}{\beta}\int_{\beta_0}^{\beta}(E - \mu x)d\beta \quad \text{with } \phi_0(\beta_0,\mu) = E - \mu x \tag{3}$$

where $\beta = \frac{1}{k_B T}$, and k_B is the Boltzmann's constant. The starting values $\phi_0(\beta_0, \mu)$ can be approximated as $E - \mu x$ because of the negligible entropy contribution at low temperature (i.e., T = 10 K).

Then at each T, ϕ was integrated by variable μ in both forward and backward directions using **Eq. 4**,

$$\phi(\beta, \mu) = \phi_0(\beta, \mu_0) - \frac{1}{\beta}\int_{\mu_0}^{\mu} x \, d\mu \quad (4)$$

with $\phi_0(\beta, \mu_0) = \phi_{heating}(\beta, \mu_0)$

the integration at each μ start from $\phi_{heating}(\beta, \mu_0)$, where μ_0 = –4.5, –3.6, –2.5 eV/f.u. for $1 \leq x \leq 3$, and 6.5, 7.2 and 9.5 eV/f.u. for $3 \leq x \leq 4$, respectively.

After the thermodynamic integration the phase boundaries were found at the intersections of grand-canonical potential envelops in the (x, T) space, which was converted from (μ, T) space. The discontinuities in x vs μ and variations of C_v vs. μ were further considered to identify the phase boundaries, as shown in **Figure S6**.

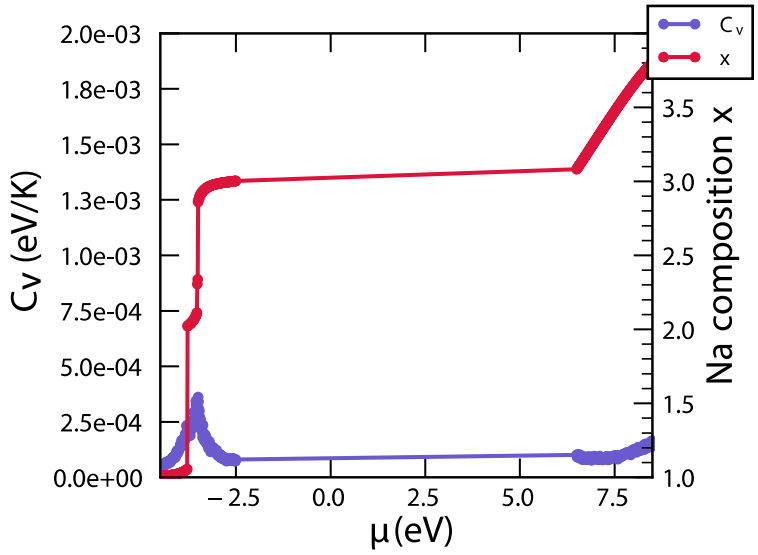

Figure S6 Variations of normalized heat capacity C_v (per f.u.) and Na composition x vs. Na chemical potential μ, at T= 680 K, obtained from gcMC. The region of –4.5 $\leq \mu \leq$ –2.5 eV/f.u. is simulated using CE model fitted for the composition range N_1VP – N_3VP, and the region of $\mu \geq$ 6.5 eV/f.u. is simulated using CE model fitted for the composition range N_3VP – N_4VP. The discontinuities of x vs. μ curve (red) indicates the stable single-phases at x = 1, 2, 3, and their relevant phase boundaries. The solid solution behavior is also shown with the continuous sloping curve at N_3VP – N_4VP region.

S3-3. Configuration entropy

Figure S7 plots the configurational entropy for Na composition region 1 ≤ x ≤ 3 generated by gcMC.

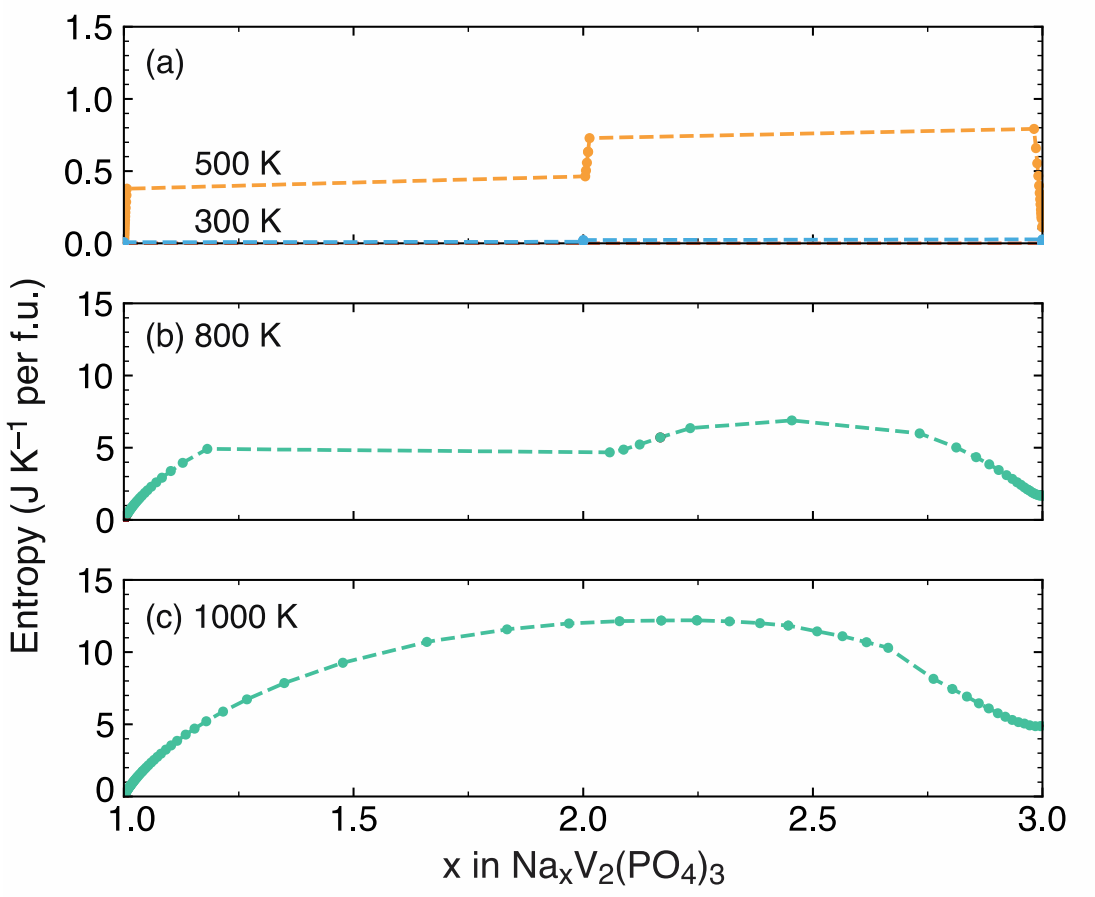

Figure S7 Computed configurational entropy S(x) obtained from gcMC simulations as a function of Na content x in N_xVP and at specific temperatures 300 K, 500 K (panel(a)), 800 K (panel(b)), and 1000 K (panel(c)).

S3-4. Computing Voltage Curves and Mixing Energies from DFT and gcMC Simulations

Reversible Na^+ insertion/extraction into/from N_xVP structure is given by **Eq. 5**.

$$Na_xV_2(PO_4)_3 + yNa^+ + ye^- - \overset{\Delta G^0}{\longleftrightarrow} Na_{x+y}V_2(PO_4)_3 \quad (5)$$

where x indicates the initial Na content and y indicates the number of inserted Na^+. ΔG^0 is the change of Gibbs free energy for the reaction of **Eq. 5**, can be approximated from DFT total energies by ignoring the zero-point energy correction, pV, and entropic effects. Notably, configurational entropic effects can be included in ΔG^0 using the statistical sampling from gcMC simulations.

The corresponding average intercalation voltage for the reaction of **Eq. 5** is derived based on ΔG^0 using **Eq. 6**.

$$V = -\frac{\Delta G^0}{yF} \approx -\frac{E\left(N_{x+y}VP\right) - [E(N_xVP) + y\mu_{Na}]}{yF} \quad (6)$$

where μ_{Na} is the Na chemical potential (set to the bulk Na metal) and F is the Faraday constant.

To evaluate the phase stability while intercalating Na^+ into the N_xVP structure, we computed the mixing energies (E_{mixing}) at different Na compositions, using **Eq. 7**, and defined with respect to the energy of N_1VP and N_4VP end-member compositions.

$$E_{mixing}(x) = E[N_xVP] - \left(\frac{4-x}{3}\right)E[N_1VP] - \left(\frac{x-1}{3}\right)E[N_4VP] \quad (7)$$

where $E[N_xVP]$, $E[N_1VP]$, and $E[N_4VP]$ are the DFT energies of a given N_xVP Na/vacancy orderings, the fully discharged (N_4VP), and the fully charged (N_1VP) structures. Note, the mixing energies can be used interchangeably with formation energies in our study. The structures with the lowest mixing energies (i.e., N_1VP, N_2VP, N_3VP, and N_4VP) were used to construct the convex hull through a convex minimization at 0 K.

Additionally, the voltage curves at different temperatures are calculated from the Na chemical potential $\mu_{Na}(x)$ of gcMC, using **Eq. 8**.

$$V(x) = -\mu_{Na}(x) + \Delta\mu_{shift} \quad (8)$$

The voltage at each Na composition is obtained by applying a chemical potential shift, $\Delta\mu_{shift}$, to $\mu_{\mathrm{Na}}(\mathrm{x})$ from the gcMC. $\Delta\mu_{shift}$ measures the difference between the DFT-derived average voltage at a specific Na composition range (i.e., 1 ≤ x ≤ 3, or 3 ≤ x ≤ 4) and the gcMC average chemical potential μ_{Na} for the same range, referenced to the structure with the least configurational entropy (since least configurational entropy ≈ negligible shift in G with T).

References

1 A. Van der Ven, J. C. Thomas, Q. Xu and J. Bhattacharya, *Math. Comput. Simul.*, 2010, **80**, 1393–1410.
2 B. Puchala and A. Van der Ven, *Phys. Rev. B*, 2013, **88**, 094108.
3 J. C. Thomas and A. V. der Ven, *Phys. Rev. B*, 2013, **88**, 214111.
4 CASM Developers, *Casmcode: V0.2.1*, Zenodo, 2017.
5 L. J. Nelson, G. L. W. Hart, F. Zhou and V. Ozoliņš, *Phys. Rev. B*, 2013, **87**, 035125.
6 K. Binder, D. Heermann, L. Roelofs, A. J. Mallinckrodt and S. McKay, *Comput. Phys.*, 1993, **7**, 156.
7 A. van de Walle and M. Asta, *Model. Simul. Mater. Sci. Eng.*, 2002, **10**, 521–538.